International Journal of Nanomedicine

Dovepress
open access to scientific and medical research

Open Access Full Text Article

ORIGINAL RESEARCH

Biosynthesis, characterization, and anticancer effect of plant-mediated silver nanoparticles using *Coptis chinensis*

Junwen Pei
Binfan Fu
Lifeng Jiang
Taizhen Sun

Department of Integrated Traditional Chinese and Western Medicine, The Henan Cancer Hospital, Affiliated Cancer Hospital of Zhengzhou University, Zhengzhou, Henan 450008, China

Background: Tremendous growth in nanotechnology has opened up new frontiers in fundamental and applied aspects, including the synthesis of nanoscale matter and understanding/utilizing its exotic physicochemical and optoelectronic properties. Green-synthesis methods employing either biological microorganisms or plant extracts have emerged as a simple and alternative to chemical synthesis.

Methods: In our present study, we aimed to synthesize silver nanoparticles (AgNPs) in combination with an aqueous extract of *Coptis chinensis* (CC) using a suitable ecofriendly green-synthesis way.

Results: In our results, ultraviolet-visible spectroscopy revealed a near-absorbance peak at 450 nm, which confirmed the AgNP synthesis. The crystalline nature of the AgNPs was revealed with X-ray diffraction. Transmission electron-microscopy analysis showed spherically dispersed nanoparticles of 6–45 nm diameter. We analyzed the elementary mechanism across A549 lung carcinoma cells ahead of treatment with doses of CC-AgNPs (10 µg/mL and 25 µg/mL). The antiproliferative effect of CC-AgNPs revealed a significant decline in cell viability. Antibacterial assays with both Gram-negative (*Escherichia coli*) and Gram-positive (*Staphylococcus aureus*) bacteria exhibited a higher zone of inhibition against *S. aureus*.

Conclusion: Furthermore, CC-AgNPs regulated apoptosis using the intrinsic pathway to inhibit A549-cell proliferation. Proliferation migration and invasion were notably inhibited by CC-AgNPs, which promoted apoptosis in lung adenocarcinoma cells by regulating the apoptotic pathway.

Keywords: *Coptis chinensis*, silver nanoparticles, antimicrobial, lung cancer, apoptosis, invasion

Introduction

Apoptosis is a metazoan sequence of action that controls cell abolition with the intention to exert an important role in embryonic amelioration and adult tissue homeostasis. In multifarious diseases, cancer occurs due to a defect in apoptosis and dysregulation.[1] In many types of cancer, a defect in apoptosis is a pervasive phenomenon, and its stimulation through intonation of apoptotic pathways with chemical agents has been shown to represent a promising approach in therapeutics of cancer.[2] Two discrete (until now interrelated) signaling pathways induce apoptosis through a core intracellular machinery of death proteases called caspases. The extrinsic pathway activates caspases via cell-surface death ligands emitting immunoeffector cells.[3] Caspases are retained by an intrinsic apoptotic pathway via members of the Bcl2-protein family members like the proapoptotic Bax, Bak, the antiapoptotic Bcl2, and BclXL, and severe cellular damage or stress responses to mitochondria can occur.[4] A number of

Correspondence: Taizhen Sun
Department of Integrated Traditional Chinese and Western Medicine, The Henan Cancer Hospital, Affiliated Cancer Hospital of Zhengzhou University, Zhengzhou, Henan 450008, China
Email stz1967@sina.com

submit your manuscript | www.dovepress.com
Dovepress
http://dx.doi.org/10.2147/IJN.S188235

pro/antiapoptotic molecules regulate apoptosis. Therefore, progress in anticancer agents targeting these molecules has become a prominent approach in cancer chemotherapy.[5] Regulation of apoptosis for the most part is an aim in anticancer therapies, in conjunction with radiotherapy, and immunochemotherapy.[6] Worldwide cancer is an important cause of mortality, accounting for up to 8.8 million deaths in 2015. Lung cancer is a universal and primary cause of cancer death worldwide. In 2018, an estimated total of 234,030 new lung and bronchus cancer cases were diagnosed, and incidence among both males (121,680 cases) and females (112,350 cases) is second highest among all cancer types.[7] Lung cancer consists mainly in squamous-cell carcinoma and adenocarcinoma.[8,9] Routine chemotherapeutic agents are used in lung cancer. Chances of survival are $<15\%$.[10] Drug resistance can develop during treatment, and currently available chemotherapy has become less sensitive. The efficiency of chemotherapy drugs and a key challenge in developing potent therapeutic agents can overcome existing chemotherapeutic limitations.

Areas of science have developed swiftly through nanotechnology. In recent years, research has focused on silver nanoparticles (AgNPs), due to their unique ocular, mechanical, electrical, and chemical properties, which are significantly diverse from those containing quantum materials. Nanotechnology additionally blocks a basic method in the advancement of unblemished, nontoxic, and ecofriendly approaches, with the key combination of herbal and silver NPs having the essential capacity of decreasing metals by particular metabolic pathways.[11] Synthesis of AgNPs is a widely used approach, eg, in solution diminution, photochemical and modulated micelle reactions, thermal decay of silver compounds, and radiation-aided sonochemical and electrochemical microwave-aided techniques. Nowadays, there is an emerging requirement to construct ecofriendly forms that do not consume dangerous chemicals in consolidation. In cancer research, AgNPs have attracted much interest because of their facile surface modification and synthesis, robustly augmentable and amenable visual properties, and superior biocompatibility.[12] Over the last decade, tremendous effort has been devoted to the combination of green chemistry and biological approaches designed for the purpose of AgNP synthesis.

Traditionally, *Coptis chinensis* (CC) Linn, known as *huanglian* in Chinese, is a plant used in Chinese medicine. The rhizome of CC Franch (Ranunculaceae) has been used in traditional medicine for relieving fidgetiness, and detoxification.[13] CC has been used widely in the treatment of various clinical conditions, due to its antidiabetic,[14] anti-inflammatory,[15] antiproliferation,[16] antioxidant,[17] antihypertension,[18] antihypoglycemic, antihypocholesterolemic,[19] and anti-Alzheimer's effects.[20]

In this study, we investigated green AgNPs synthesized from CC confirmed by ultraviolet (UV) light, X-ray diffraction (XRD), scanning electron microscopy (SEM), and Fourier-transform infrared (FTIR) spectroscopy, and their anticancer activity was studied in A549 cells, in addition to evaluation of antibacterial and antimicrobial activities. Regulation of apoptosis with CC-AgNPs is a dynamic region of research in modern experiments to discover more effective therapy for cancer treatment. CC-AgNP-regulated apoptosis is complicated and involves unraveled mechanisms. Here, we used CC to build on recent advances. Recently, therapeutic settings were induced by CC through apoptosis. We focused on the challenges of using CC as a potential substitute option for cancer therapy.

Methods

Chemicals

RPMI 1640 medium, dimethyl sulfoxide, antibiotic/antimycotic (100×) solution, ampicillin, trypsin–EDTA (0.25%), penicillin–streptomycin–amphotericin, and FBS were purchased from Thermo Fisher Scientific (Waltham, MA, USA). A protein-estimation kit, acrylamide, ammonium persulfate, tetramethylethylene diamine, and prestained SDS-PAGE standard were from Bio-Rad (Hercules, CA, USA) and an enhanced chemiluminescence kit was procured from Thermo Fisher Scientific. Polyvinylidene difluoride membrane was procured from EMD Millipore (Billerica, MA, USA). All antibodies used in this study were purchased from Santa Cruz Biotechnology (Dallas, TX, USA).

Preparation of CC-leaf extract

CC leaves were washed with distilled water, then cut into small pieces. These pieces were dried in an oven at 40°C for 2 days. The dried leaves were then finely ground into powder, stored in amber glass bottles, and kept at low temperature for further analysis. CC powder (20 g) was extracted with methanol using a Soxhlet apparatus. This extract was filtered using Whatman filter paper grade 1 with a vacuum pump. The solvent was completely removed at 40°C in a rotary vacuum evaporator. At 4°C, the concentrated abstract was stored in dark bottles until used.

Preparation of silver nitrate solution

Silver nitrate (0.75 Mm) solutions were freshly prepared using 100 cm^3 distilled water. For biosynthesis of NPs, in a

conical flask, about 50 cm^3 0.75 Mm $AgNO_3$ was taken and 20 cm^3 of the extract added to it drop by drop. The aforementioned solution was kept on a magnetic stirrer.

Synthesis of silver nanoparticles

Methanolic CC extract (15 mL) and an aqueous solution of 0.75 mM $AgNO_3$ were mixed together. This blend was incubated at room temperature in dark conditions. Development/formation of NPs was visualized by color transition.

Cells and cell culture

Non-small cell lung carcinoma cell lines (A549) were purchased from the Institute of Biochemistry and Cell Biology, Chinese Academy of Sciences (Shanghai, China). A549 cancer cells were grown in RPMI 1640 medium at 37°C in a 5% CO_2 atmosphere. Cells were supplemented with 10% FBS. Potassium penicillin (100 U) and 100 µg streptomycin sulfate/1 mL was added in a culture medium.

Characterization techniques

UV-visible (UV-vis) absorbance was used to monitor the development of AgNPs. Crystalline AgNPs were examined by XRD. All XRD and dynamic light scattering (DLS) data were pooled under the same experimental conditions. FTIR spectra for CC extracts were obtained in the range 4,000–400 cm^{-1} using the KBr-pellet method. SEM was used to analyze AgNPs.

MTT assays

Newly grown A549 cells were treated for 72 hours, then incubated at 37°C in a 5% CO_2 atmosphere. Cell-viability assays were carried out using the standard MTT method, while final absorbance was measured at a wavelength of 570 nm.

Cell-migration and -invasion assays

Cells were grown in transwell chambers at a concentration of 10^5 cells/100 µL and treated with different concentrations (10 µg/mL, 25 µg/mL) of CC-AgNPs. After 24 hours, upper-surface cells were removed. These cells were invaded or had migrated. Then, cells were stained and visualized using high-power microscopy and counted. After 24 hours, cells were fixed with 40% polyoxymethylene, washed with PBS, then incubated with Hoechst 33258 (10 µg/mL) in the dark for 5 minutes. After staining, cells were visualized by fluorescence microscopy.

TUNEL assays

DNA-fragmentation studies were used to detect apoptosis. Based on the TUNEL reaction, the presence of apoptotic DNA fragments was analyzed by fluorescence detection. To examine nuclei, total cell numbers were labeled as colocalized dye using DAPI. Image was observed with fluorescence microscopy at 100× magnification.

Cell-proliferation assays

CC-AgNPs were added to make final concentrations of 10 and 20 µg/mL. Before that, A549 cells were inoculated in 96-well plates with 10^4 cells per well. MTT (10 µL 5 mg/mL) was added to each well at 12, 24, 36, 48, and 72 hours, followed by 4 hours' incubation. Then, 200 µL dimethyl sulfoxide was added and incubated for 10 minutes. Optical density values at 570 nm in each group of cells were measured using a microplate reader. IC_{50} values for CC were calculated for further molecular analysis.

Western blot analysis

After treatment, cells were washed twice using ice-cold PBS and 200 µL lysis buffer used to lyse the cells. Then, cells were kept on ice for 5 minutes and lysates gathered using a cell scraper, pipetted, and cells pooled then centrifuged at 1,000 rpm for 10 minutes. The clear supernatant was further stored at 80°C. Total protein was quantified using the Bradford protein assay. To perform SDS-PAGE, equal amounts of 10–20 mg of protein were used. After electrophoretic separation, proteins were transferred to polyvinylidene difluoride membranes by a semidry method within 30 minutes. TBS-T 3% was used for blocking for about 1 hour and incubated with primary antibodies for 24 hours in 4°C. Finally, after being washed, secondary antibodies were added to membranes for 1 hour to react with primary antibodies. Primary antibodies – anti-Bax, mouse anti-β-actin, and mouse anti-Bcl2 – and goat secondary antibodies were used.

Statistical analysis

Data are presented as means and SE from experiments, each performed in triplicate. Statistical significance was evaluated by two-sided Student's *t*-tests. $P<0.05$ was considered significant.

Results

UV-vis spectra analysis

The fundamental system of UV-vis spectroscopy was used to determine the primary existence of AgNPs in liquid medium. Color change demonstrated the presence of AgNPs. UV-vis spectra were further considered and observed by taking readings for various durations. UV-vis spectra of AgNP

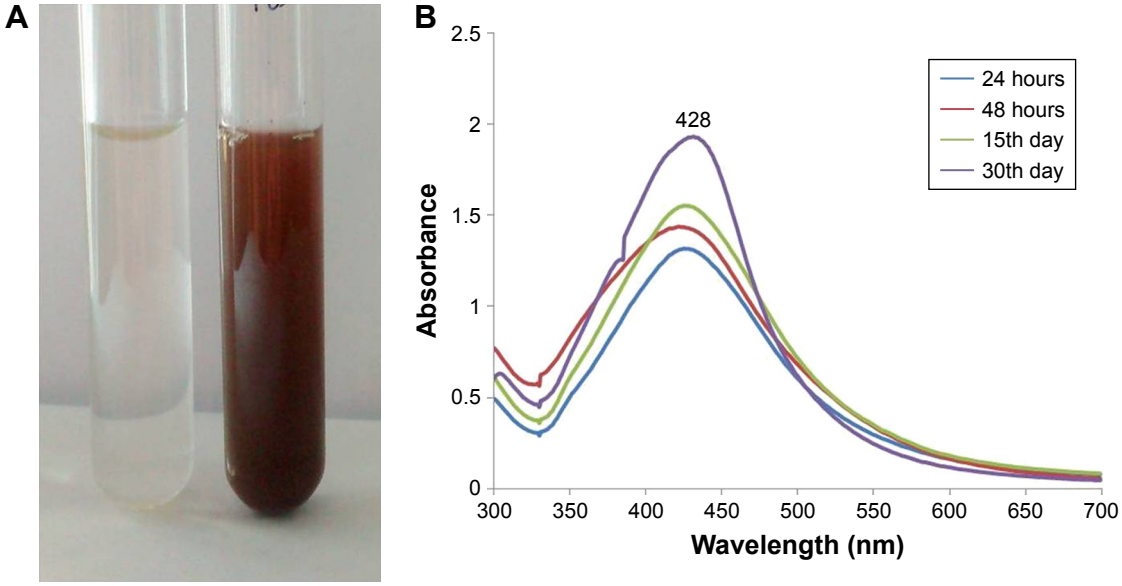

Figure 1 Ultraviolet-visible absorption pattern of AgNPs synthesized from *Coptis chinensis* (CC).
Notes: (**A**) Synthesized CC-AgNPs; (**B**) ultraviolet-visible spectra of synthesized CC-AgNPs.
Abbreviation: AgNPs, silver nanoparticles.

formation using CC-AgNP extract revealed absorption peaks at 24 hours, 48 hours, 15 days, and 30 days in aqueous medium. The medium is shown in Figure 1A. Peaks showing spectral lines were observed (Figure 1B). Surface plasma resonance of silver colloids for diverse duration was observed around 428 nm.

X-ray diffraction

The crystalline nature of particles was verified by XRD. XRD patterns showed face-centered cubic silver structure indexed by Bragg's reflections. AgNP XRD pattern was recorded at 30°–70° at two angles. High-intensity peaks from XRD patterns depicted peaks at around 37°, 44°, and 64°, corresponding to three diffraction faces of silver. The XRD peak at around 37° represented the Bragg reflection corresponding to the (111) plane (Figure 2A). The presence of biological material in free state might crystallize independently leading to Bragg reflections.

Dynamic light scattering

Size of synthesized AgNPs was determined by DLS. DLS reveals the size of colloidal scattering using the radiance of a molecule suspension undergoing Brownian motion by a laser beam. Particle-size distribution is analyzed with DLS. Based on the results, the mean diameter of AgNPs in optimum conditions was 135.8 nm (Figure 2B).

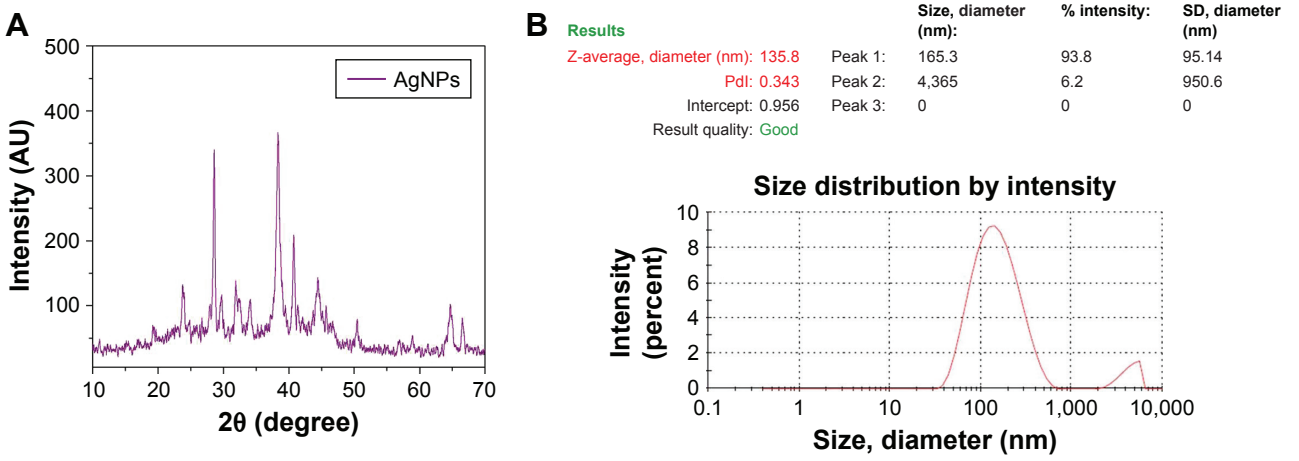

Figure 2 X-ray diffraction (**A**) and dynamic light scattering (**B**) of silver nanoparticles synthesized from *Coptis chinensis*.

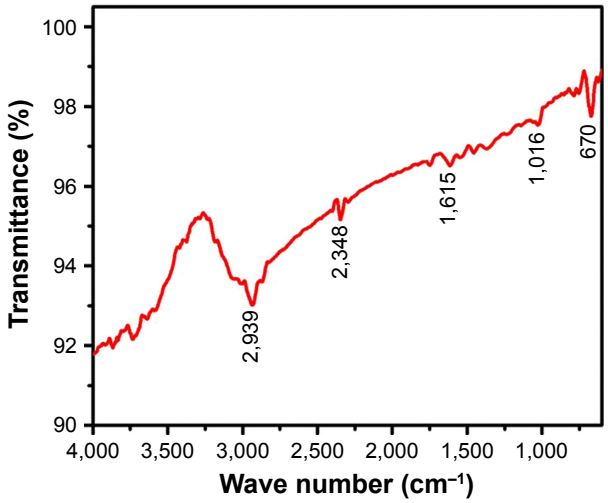

Figure 3 Fourier-transform infrared-spectroscopy analysis of silver nanoparticles synthesized from *Coptis chinensis*.

Fourier-transform infrared spectroscopy

FTIR spectra of AgNPs demonstrated peaks at 2,939, 2,348, 1,615, 1,016, and 670 cm^{-1} (Figure 3). New-bond formation in a reacting solution is revealed by FTIR spectra. The active compounds in CC-AgNPs showing specific bands corresponding to the reacting molecules were specified by spectra. The functional groups of CC extract display an array of absorption peaks, depicting complexity. The strong absorption peak at 2,939 cm^{-1} was assigned to –CH stretching vibrations of $-CH_3$ and $-CH_2$ functional groups. The peak at 2,348 cm^{-1} was assigned to the C=O group of carboxylic acids. The peak at 1,615 cm^{-1} indicates the CO, C–O, and O–H groups. The intense band at 1,016 cm^{-1} can be assigned to C–N stretching vibrations of aliphatic amines. FTIR study indicated that the carboxyl (–C=O) and hydroxyl (–OH) groups of CC extract played crucial roles in the reduction of Ag^+ to AgNPs.

Scanning electron microscopy and energy-dispersive X-ray analysis

AgNP morphology was observed as a smooth spherical surface. The shape of the particles was determined by SEM. Slightly agglomerated powder-form particles were revealed by microscopy (Figure 4A). The chemical composition of CC-AgNPs was analyzed using energy-dispersive X-rays, the spectrum of which (Figure 4B) illustrated that the layer around AgNPs was comprised mainly of C and Ag.

Antimicrobial assays

Both Gram-negative and Gram-positive bacteria – *Klebsiella pneumoniae*, *Pseudomonas aeruginosa*, *Bacillus subtilis*, *Staphylococcus aureus*, and *Aspergillus niger* fungi – were tested to analyze the antimicrobial effect of AgNPs. Various concentrations of AgNPs with microorganism antibacterial activities are illustrated in Figure 5. The numerical value of the inhibition zone and the control antibiotics fluconazole and streptomycin are given in Table 1. The synthesized

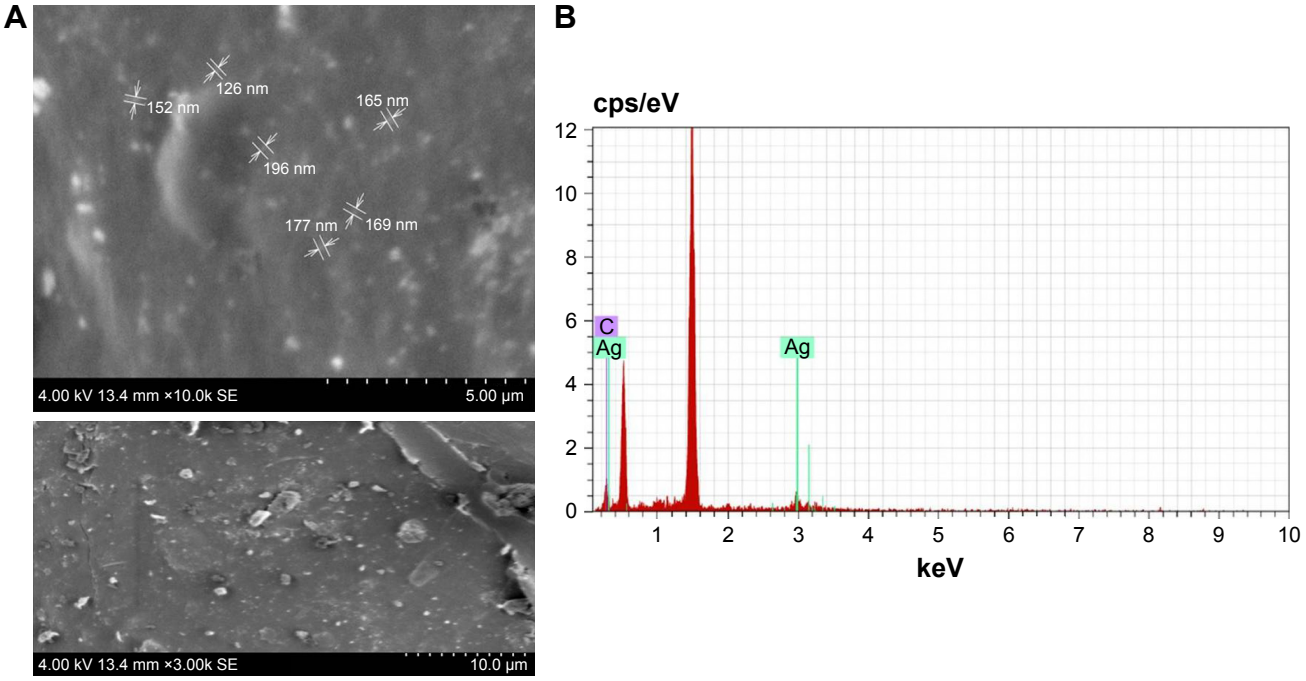

Figure 4 Scanning electron microscopy (**A**) and energy dispersive X-ray analysis (**B**) of silver nanoparticles synthesized from *Coptis chinensis*.

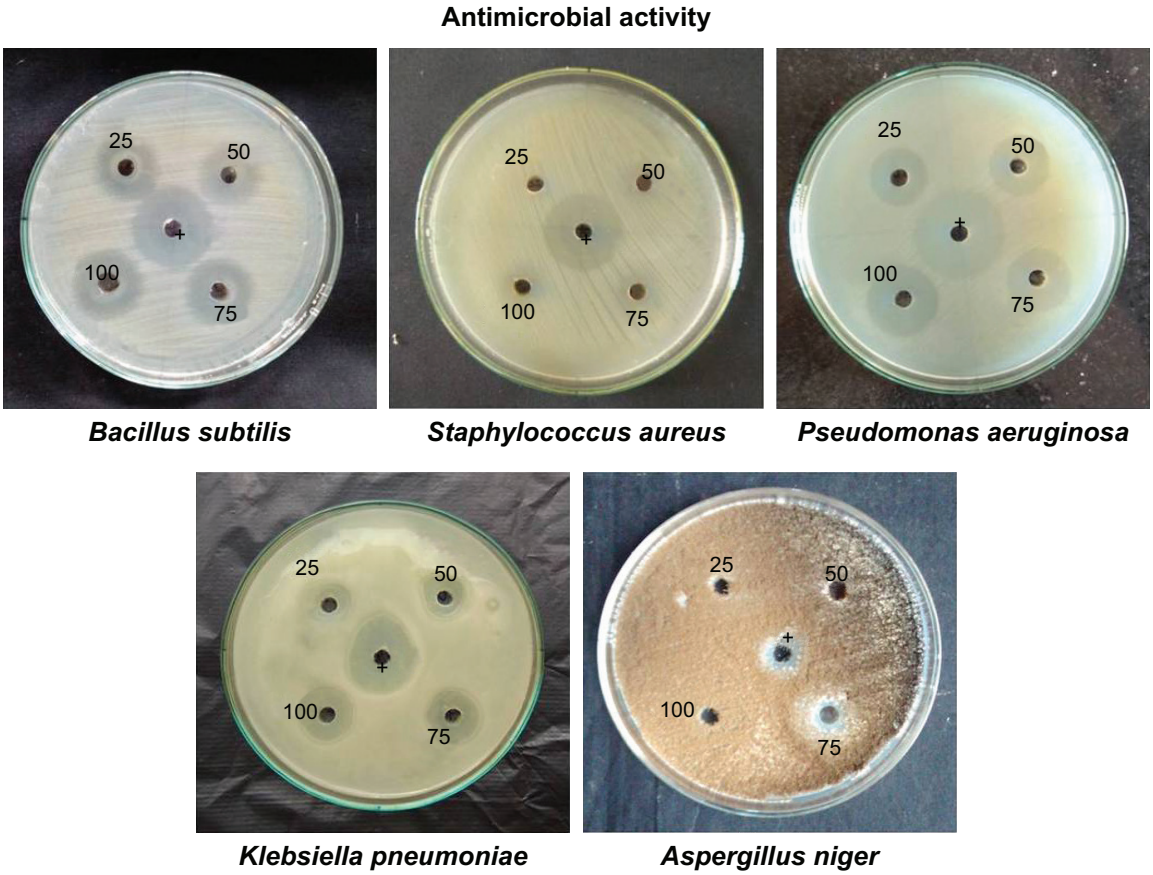

Figure 5 Antimicrobial activity of silver nanoparticles synthesized from *Coptis chinensis*.
Note: +Streptomycin and fluconazole.

CC-AgNPs restrained microorganism growth. Zone values were observed for the synthesized CC-AgNPs against five different microorganisms. The results showed more activity on *B. subtilis* and less effect on *A. niger* with increasing (25, 50, 75, and 100 µL/mL) concentrations of AgNPs. AgNPs were responsible for the release of diffusible inhibitory compounds from bacterial walls during incubation. These CC-AgNPs have applications in cancer therapeutics by virtue of wound-healing functions and antimicrobial activity. Green synthesis of CC-AgNPs has also paved the pathway for better therapeutic effects in the medical field.

Anticarcinogenic effect of CC-AgNPs

The cytotoxic activity of CC-AgNPs was estimated with MTT assays. After 24 hours' incubation, the non-small-cell lung carcinoma cell line (A549) treated with different concentrations of CC-AgNPs (0, 5, 10, 15, and 20 µg/mL) showed decreased percentages of viable cells (Figure 6). This proves that the CC-AgNPs were cytotoxic to cancer cells.

TUNEL assays

DNA fragmentation is widely used to measure typical apoptosis features. Two factors confirm the initiation of apoptosis – faltering and decreased cell size – with cell volumes reduced and shrunken. Cultured cells could harvest diverse biochemical and molecular pattern changes in AgNPs. For instance, TUNEL assays detected AgNP-induced DNA breakage in cell lines. Treatment of A549 cells with CC-AgNPs (10 µg/mL) and AgNPs (25 µg/mL) exposed a noteworthy manifestation of positively labeled cells and expressive apoptotic DNA fragmentation (Figure 7). In control cultures, few apoptotic-like cells were observed. CC-AgNPs mediated migration and invasion of A549 cells.

Effect of CC-AgNPs on cancer-cell invasion and migration

Transwell assays were performed to assess the effect of CC-AgNPs on A549-cell invasion and migration (Figure 8), which are the hallmarks of cancer progression. CC-AgNPs exhibited

Table 1 Antibacterial activity of silver nanoparticles (AgNPs) from *Coptis chinensis*

Sample code	Zone of inhibition (mm) and minimum inhibitory concentration (μg/mL)											
	Bacillus subtilis				*Staphylococcus aureus*				*Klebsiella pneumoniae*			
	25 μL	50 μL	75 μL	100 μL	25 μL	50 μL	75 μL	100 μL	25 μL	50 μL	75 μL	100 μL
AgNPs	14	14	16	18	6	7	10	12	8	9	11	13
Streptomycin (10 μg)	20				23				19			
Not active												
	25				50				75			
	–				–				–			
	Fluconazole				12							

Sample code	Pseudomonas aeruginosa			
	25 μL	50 μL	75 μL	100 μL
AgNPs	12	12	14	16
Streptomycin (10 μg)	24			
Not active				
	100			
	11 mm			

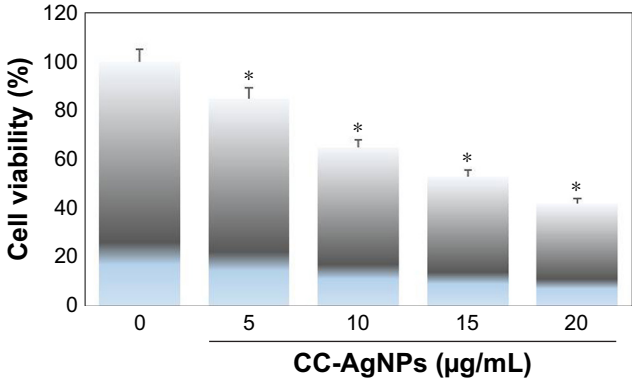

Figure 6 Cytotoxicity effect by MTT assay of silver nanoparticles (AgNPs) synthesized from *Coptis chinensis* (CC) on lung alveolar carcinoma cell lines.
Notes: Normal human non-small-cell lung carcinoma cells (A549) were exposed to different concentrations of CC-AgNPs for 24 hours and the effect on cell viability analyzed by MTT assay. The number of viable cells after treatment is expressed as a percentage of the vehicle-only control. This experiment was repeated thrice, and bars represent SE (*$P<0.05$).

significant inhibition of both cell-invasion and -migration properties of A549 when compared to 5 μg/mL CC-AgNPs in 10 μg/mL-treated groups, which showed high rates of cell invasion and migration.

Antiapoptotic effect of CC-AgNPs on lung alveolar carcinoma (A549) cell line

To determine CC-AgNP mechanisms in cell death, immunoblot analysis was used to identify apoptotic proteins, revealing the regulation of proapoptotic and antiapoptotic proteins in a dose-dependent manner. CC-AgNPs at 10 μg/mL were more effective than 5 μg/mL, showing that the higher concentration was more efficient in regulating apoptosis (Figure 9). This indicated regulation of Bax, Bcl2, and caspase 3, BclXL, revealing that the proapoptotic protein caspase 3 and Bax were significantly upregulated, while the antiapoptotic protein BclXL was significantly downregulated ($P<0.05$). In our study, β-actin was used as a control.

Discussion

The preparation of silver and herbal combinations for modern drug formulation and delivery deploys the antique theory of Ayurvedic medicine. AgNPs are becoming more useful, specifically for cancer treatment.[21] CC-AgNPs show high antibacterial activity against both Gram-positive and -negative bacteria. The nuclear content of bacteria enables AgNPs to reach them easily. The size and large surface area of the AgNPs can be attributed to high antibacterial activity. Neither $AgNO_3$ solution nor CC extract shows any zone of

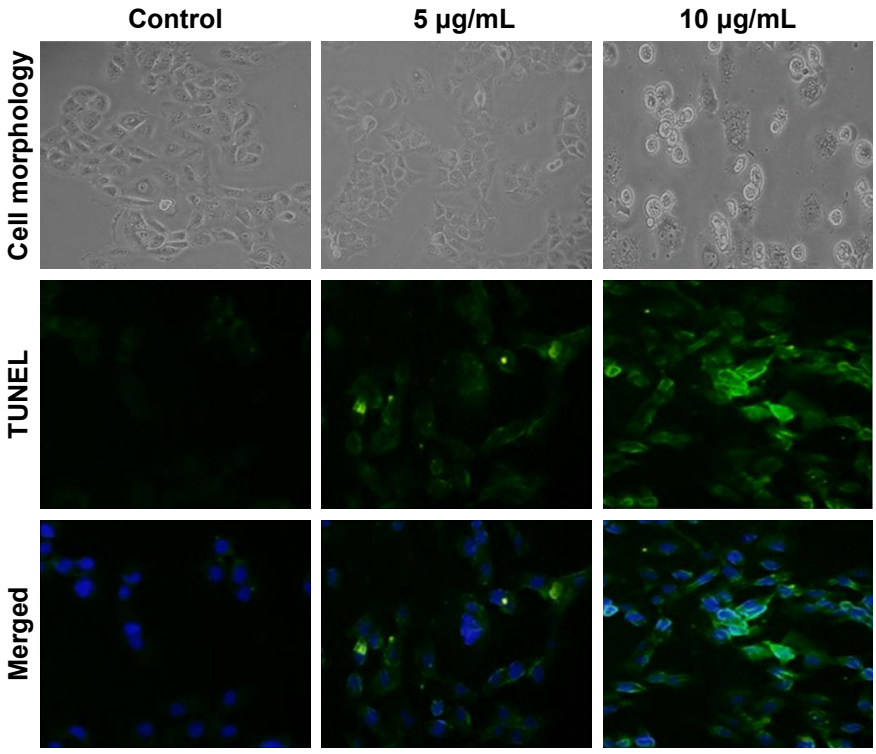

Figure 7 Effect of silver nanoparticles (AgNPs) synthesized from *Coptis chinensis* (CC) on lung alveolar carcinoma (A549)-cell morphology and TUNEL assay.
Notes: A549 cells were incubated with 5 and 10 µg/mL CC-AgNPs for 24 hours. Microscopy representative of three independent experiments.

inhibition from selected bacterial strains. $AgNO_3$ at selected concentrations symbolizes the antibacterial potential of extracts. The erratic release of deficient concentrations of silver ions from $AgNO_3$ may be a cause of its prohibition efficiency of antimicrobial agents. It suggests attachment of AgNPs on surfaces of bacterial cell membranes, thereby releasing silver ions that can disrupt permeability of the cell membrane and bacterial DNA replication.[22]

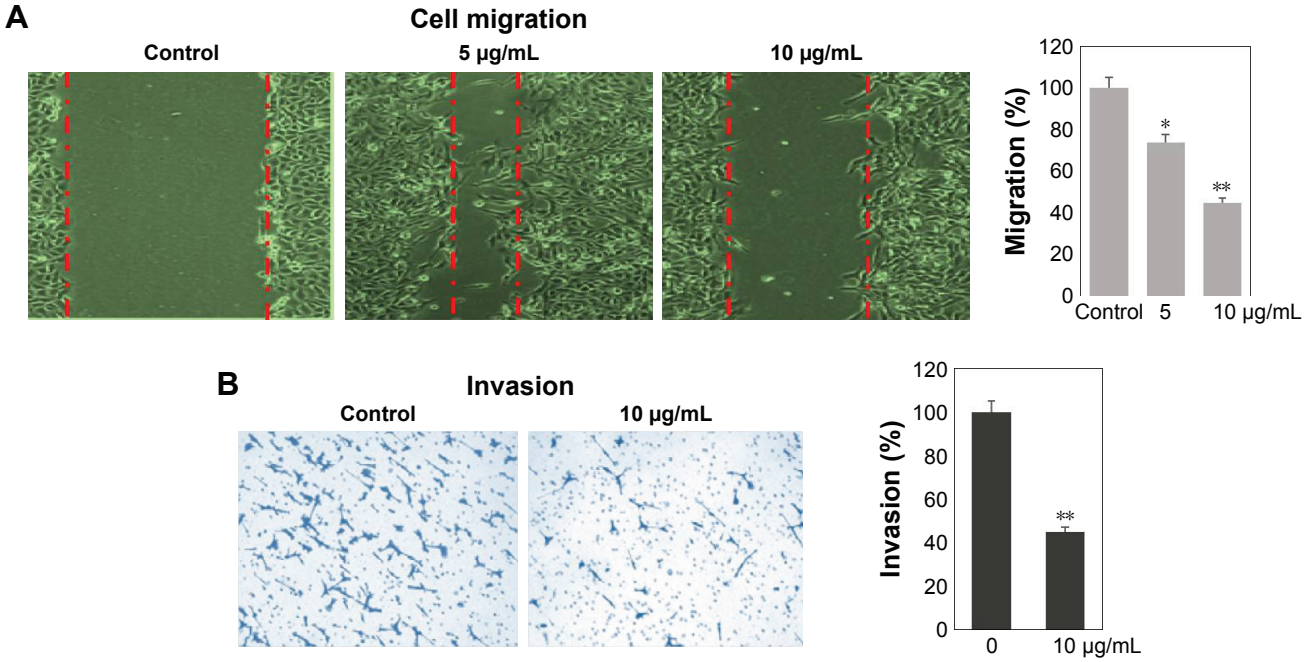

Figure 8 Effect of silver nanoparticles (AgNPs) synthesized from *Coptis chinensis* (CC) on lung alveolar carcinoma (A549) cell-line migration and invasion.
Notes: (**A**) Migration fold represented in graph bars; (**B**) A549 cells were incubated with 10 µg/mL CC-AgNPs, and invasion fold is represented in graph bars. * and ** represents statistical significance between control vs other groups at $P<0.05$ and $P<0.01$ respectively, using Dunnett's test.

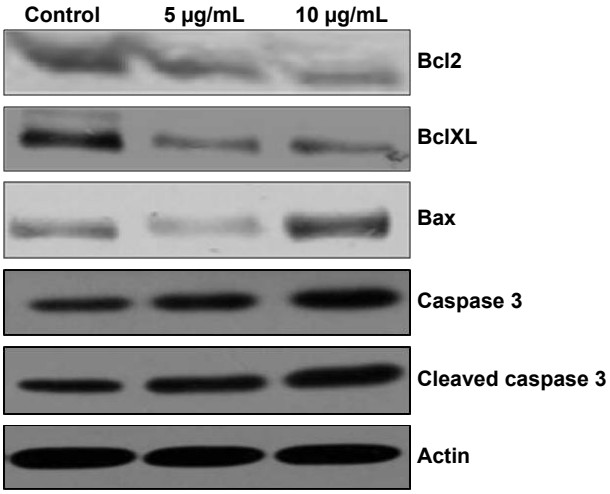

Figure 9 Antiapoptotic effect of silver nanoparticles (AgNPs) synthesized from *Coptis chinensis* (CC) on lung alveolar carcinoma (A549) cell line.
Notes: A549 cells were treated with CC-AgNPs (5 and 10 µg) for 24 hours, and dose-dependent changes in Bcl2, Bax, BclXL, and caspase 3 expression were monitored by Western blotting, with β-actin as loading control.

In addition, NPs acquired a large exterior area that afforded immensely better contact and interaction. Worldwide lung cancer is the major cause of cancer mortality in human beings.[23] Great achievements have been realized by incorporating AgNPs with cancer treatments. They intensely mediate cell functions that are regulated by molecular processes, but they cannot interact spontaneously with cells.[24] This study examined the synergistic effects that CC-AgNPs could deploy on lung cancer-cell apoptosis. This study demonstrated that human lung adenocarcinoma (A549 cells) exerted an anticancer consequence in alliance with CC-AgNPs by the regulation of apoptosis. Anticancer and antiproliferative effects of CC-AgNPs against A549 cells included growth inhibition in a dose-dependent manner, which showed selectivity for tumor cells. Additionally, intrinsic or extrinsic pathways of apoptosis induced by AgNPs have been demonstrated in several studies.[25–28]

Mitochondrial and proapoptotic proteins mediate the intrinsic apoptotic pathway,[29,30] and our results clearly indicate that apoptosis was induced by CC-AgNPs via involvement of a mitochondria-mediated pathway in A549 cells. Subsequent apoptosis and loss of mitochondrial membrane potential is mediated by the Bcl2 protein family. This family is divided into two classes based on Bcl2 homology: the proapoptotic Bak and Bax, and the antiapoptotic Bcl2 and BclXL.[31,32] In the present study, Bcl2 levels were remitting after treating A549 cells with CC-AgNPs, whereas proapoptotic proteins reminiscent of caspase 3 and Bax were unregulated. Cell divergence, shape, and mechanical properties of the plasma membrane were determined by the chief constituent actin, a prominent filament in the plasma membrane allied with the cytoskeleton.[33] Apoptosis relationships and actin-filament interruption have been reported in several studies.[34] In this study, actin levels were not altered by the circumstances of the cell. This is the major reason to use β-actin as control. We also established Bax and caspase 3 upregulation and downregulation of Bcl2.

This study shows the potential of such results as downregulation of BclXL and upregulation of Bax in the treatment of A549 cells with CC-AgNPs. This observation could explain the fact that altering Bcl2 regulation is enough to affect cell susceptibility and apoptosis in A549 cell line, due to unaltered expression of Bcl2. Expression of the antiapoptotic protein BclXL was also downregulated by CC-AgNPs. Overexpression of Bcl2 is usually associated with various cancers, as well as drug resistance during chemotherapy.[35]

Conclusion

Cheap pollutant-free and ecofriendly green synthesis was used as an alternative to chemical methods for CC-AgNPs. These synthesized CC-AgNPs showed antibacterial activity on both Gram-negative and -positive bacteria. CC-AgNPs inhibited A549-cell proliferation in apoptosis regulation via the intrinsic pathway. Activation of the apoptotic pathway was accompanied by downregulation of BclXL and Bax upregulation, resulting in the inhibition of mitochondrial membrane potential. In addition, independent caspase 3 cell death was found in response to treatment of A549 cells with CC-AgNPs, suggesting a novel mechanism: underlying regulation of apoptosis by CC-AgNPs in lung cancer cells. CC-AgNPs significantly restrained proliferation and migration, but also promoted apoptosis in lung adenocarcinoma cells by regulation of the apoptotic pathway. The findings suggest that biogenic CC-AgNPs offer an alternative approach to overcome several limitations of chemotherapy.

Acknowledgment

This study was supported by the Henan Science and Technology Research Project (152102310159).

Disclosure

The authors report no conflicts of interest in this work.

References

1. Li-Weber M. Targeting apoptosis pathways in cancer by Chinese medicine. *Cancer Lett*. 2013;332(2):304–312.
2. von Schwarzenberg K, Vollmar AM. Targeting apoptosis pathways by natural compounds in cancer: marine compounds as lead structures and chemical tools for cancer therapy. *Cancer Lett*. 2013;332(2):295–303.
3. Lin X, Liu M, Hu C, Liao DJ. Targeting cellular proapoptotic molecules for developing anticancer agents from marine sources. *Curr Drug Targets*. 2010;11(6):708–715.

4. Constantinou C, Papas KA, Constantinou AI. Caspase-independent pathways of programmed cell death: the unraveling of new targets of cancer therapy? *Curr Cancer Drug Targets*. 2009;9(6):717–728.
5. Hardwick JM, Chen YB, Jonas EA. Multipolar functions of BCL-2 proteins link energetics to apoptosis. *Trends Cell Biol*. 2012;22(6): 318–328.
6. Karpel-Massler G, Westhoff MA, Kast RE, et al. Simultaneous interference with her1/egfr and rac1 signaling drives cytostasis and suppression of survivin in human glioma cells in vitro. *Neurochem Res*. 2017;42(5):1543–1554.
7. Siegel RL, Miller KD, Jemal A. Cancer statistics, 2018. *CA Cancer J Clin*. 2018;68(1):7–30.
8. Li C, Hong W. Research status and funding trends of lung cancer biomarkers. *J Thorac Dis*. 2013;5(5):698–705.
9. Zakowski MF. Cytology nomenclature and 2015 World Health Organization classification of lung cancer. *Cancer Cytopathol*. 2016; 124(2):81–88.
10. Siegel R, Naishadham D, Jemal A. Cancer statistics, 2013. *CA Cancer J Clin*. 2013;63:11–30.
11. Wang Y, Herron N. Nanometer sized semiconductor clusters: materials synthesis, quantum size effects & photo physical properties. *J Physical Chemistry*. 1992;96:525–532.
12. Liu B, Li W, Chang Y, Dong W, Ni L. Extraction of berberine from rhizome of Coptis chinensis Franch using supercritical fluid extraction. *J Pharm Biomed Anal*. 2006;41(3):1056–1060.
13. Jung HA, Yoon NY, Bae HJ, Min BS, Choi JS. Inhibitory activities of the alkaloids from Coptidis Rhizoma against aldose reductase. *Arch Pharm Res*. 2008;31(11):1405–1412.
14. Schinella GR, Tournier HA, Prieto JM, Mordujovich de Buschiazzo P, Ríos JL. Antioxidant activity of anti-inflammatory plant extracts. *Life Sci*. 2002;70(9):1023–1033.
15. Tse WP, Che CT, Liu K, Lin ZX. Evaluation of the anti-proliferative properties of selected psoriasis-treating Chinese medicines on cultured HaCaT cells. *J Ethnopharmacol*. 2006;108(1):133–141.
16. Yokozawa T, Satoh A, Cho EJ, Kashiwada Y, Ikeshiro Y. Protective role of Coptidis Rhizoma alkaloids against peroxynitrite-induced damage to renal tubular epithelial cells. *J Pharm Pharmacol*. 2005;57(3):367–374.
17. Ko WH, Yao XQ, Lau CW, et al. Vasorelaxant and antiproliferative effects of berberine. *Eur J Pharmacol*. 2000;399(2–3):187–196.
18. Yuan L, Tu D, Ye X, Wu J. Hypoglycemic and hypocholesterolemic effects of Coptis chinensis franch inflorescence. *Plant Foods Hum Nutr*. 2006;61(3):139–144.
19. Jung HA, Min BS, Yokozawa T, Lee JH, Kim YS, Choi JS. Anti-Alzheimer and antioxidant activities of Coptidis Rhizoma alkaloids. *Biol Pharm Bull*. 2009;32(8):1433–1438.
20. Ilango KV, Kanimozhi CV, Balaji G. Antidiabetic, antioxidant and antibacterial activities of leaf extracts of Adhatoda zeylanica. *Medic (Acanthaceae)*. *J Pharm Sci Res*. 2009;1:67–73.
21. Arachchige MC, Reshetnyak YK, Andreev OA. Corrigendum to advanced targeted nanomedicine. *J Biotechnol*. 2015;202:88–97.
22. Lu J, Zhang X, Shen T. Epigenetic profiling of H3K4Me3 reveals herbal medicine Jinfukang-induced epigenetic alteration is involved in anti-lung cancer activity. *Evid Based Complement Alternat Med*. 2016;7276161.
23. Siegel R, Ma J, Zou Z, Jemal A. Cancer statistics, 2014. *CA Cancer J Clin*. 2014;64(1):9–29.
24. Wei L, Lu J, Xu H, Patel A, Chen ZS, Chen G. Silver nanoparticles: synthesis, properties, and therapeutic applications. *Drug Discov Today*. 2015;20(5):595–601.
25. Shimizu K, Das SK, Hashimoto T, et al. Artepillin C in Brazilian propolis induces G(0)/G(1) arrest via stimulation of Cip1/p21 expression in human colon cancer cells. *Mol Carcinog*. 2005;44(4):293–299.
26. Ma DD, Yang WX. Engineered nanoparticles induce cell apoptosis: potential for cancer therapy. *Oncotarget*. 2016;7(26):40882.
27. Aso K, Kanno S, Tadano T, Satoh S, Ishikawa M. Inhibitory effect of propolis on the growth of human leukemia U937. *Biol Pharm Bull*. 2004;27(5):727–730.
28. Sawicka D, Car H, Borawska MH, Nikliński J. The anticancer activity of propolis. *Folia Histochem Cytobiol*. 2012;50(1):25–37.
29. Shan M, Fan TJ. Cytotoxicity of carteolol to human corneal epithelial cells by inducing apoptosis via triggering the Bcl-2 family protein-mediated mitochondrial pro-apoptotic pathway. *Toxicol In Vitro*. 2016;35:36–42.
30. Czabotar PE, Lessene G, Strasser A, Adams JM. Control of apoptosis by the BCL-2 protein family: implications for physiology and therapy. *Nat Rev Mol Cell Biol*. 2014;15(1):49–63.
31. Jeng PS, Inoue-Yamauchi A, Hsieh JJ, Cheng EH. BH3-Dependent and independent activation of BAX and BAK in mitochondrial apoptosis. *Curr Opin Physiol*. 2018;3:71–81.
32. Siddiqui WA, Ahad A, Ahsan H. The mystery of BCL2 family: Bcl-2 proteins and apoptosis: an update. *Arch Toxicol*. 2015;89(3): 289–317.
33. Zuccala ES, Satchwell TJ, Angrisano F, et al. Quantitative phospho-proteomics reveals the Plasmodium merozoite triggers pre-invasion host kinase modification of the red cell cytoskeleton. *Sci Rep*. 2016;6:19766.
34. Wang X, Nichols L, Grunz-Borgmann EA, et al. Fascin2 regulates cisplatin-induced apoptosis in NRK-52E cells. *Toxicol Lett*. 2017;266: 56–64.
35. Maurmann L, Belkacemi L, Adams NR, Majmudar PM, Moghaddas S, Bose RN. A novel cisplatin mediated apoptosis pathway is associated with acid sphingomyelinase and FAS proapoptotic protein activation in ovarian cancer. *Apoptosis*. 2015;20(7):960–974.